# Hydrogen Energy Storage System in a Multi–Technology Microgrid: technical features and performance

Angelo Bovo[a], Nicola Poli[b,c], Massimo Guarnieri[b,c,*]

[a]Veritas SpA, via Porto di Cavergnago 99, 30173 Venice, Italy

[b]Department of Industrial Engineering, University of Padua, via Gradenigo 6a, 35131 Padova, Italy

[c]Interdepartmental Centre Giorgio Levi Cases for Energy Economics and Technology, University of Padua, via Gradenigo 6a, 35131 Padova, Italy

*corresponding author, email: massimo.guarnieri@unipd.it , tel. +390498277524

author emails: a.bovo@gruppoveritas.it, nicola.poli@unipd.it, massimo.guarnieri@unipd.it

**Abstract**

The features and performance of a hydrogen energy storage system included in the microgrid powering a plant for advanced green technologies is presented. The microgrid is powered by a 730–kW photovoltaic source and four energy storage systems. The hydrogen storage system consists of a water demineralizer, a 22.3–kW alkaline electrolyzer generating hydrogen, its AC–DC power supply, 99.9998% hydrogen purifier, 200–bar compressor, 200–L gas storage cylinders, a 33–kW proton–exchange–membrane fuel cell running on hydrogen, its DC–AC power conditioning system. The whole system is housed in three containers provided with anti–salt filters to remove brine. The whole system is controlled by the microgrid system supervisor. Operative tests at nominal power show that the round-trip efficiency of the hydrogen energy storage system, is 8.7% with in pure electric operation and about 20.1% in a heat cogeneration operation.

**Keywords**: Energy storage system, hydrogen storage system, electrolyzer, fuel cell, microgrid

**Acronyms**

| | |
|---|---|
| AEL | Alkaline electrolyzer |
| CHC | Catalytic hydrogen combustion |
| CHP | Combined heat and power |
| CSU | Compression and storage unit |
| DOD | Deep of discharge |
| EGU | Electric generation unit |
| EL | Electrolyzer |
| ELU | Electrolyzer unit (including power supply PS) |
| EMS | Energy Management System |
| ESS | Energy storage systems |
| FC | Fuel cell |
| FCU | Fuel cell unit (including inverter INV) |
| HESS | Hydrogen energy storage system |
| HGU | Hydrogen generation unit |
| INV | Fuel cell DC/AC inverter, constituting the PCS |
| LHV | Lower heating value |
| PCS | Power conditioning system (made with INV) |
| PEMFC | Proton–exchange membrane fuel cell |
| PFR | Plug flow reactor |
| PLC | Programmable logic controller |
| PMS | Power Management Systems |
| PS | Electrolyzer AC/DC power supply |
| PSA | Pressure swing adsorption |
| PV | Photovoltaic system |
| RES | Renewable energy sources |
| RTE | Round trip efficiency |
| SOC | State of charge |
| SOFC | Solid oxide fuel cell |

## 1. Introduction

Until the 1990s, electricity grids were of the “hierarchic” type, meaning that energy was produced in large power plants and transmitted over distances (often long distances) to the final users [1–3]. This approach causes large concentrations of pollution, if the power plant run on fossil fuels, and losses along transmission lines [4,5]. Today, the need for mitigating climate change, claimed in several occasions as at the COP26 conference in Glasgow in Fall 2021 [6] and the concern on limited access to strategic fossil energy commodities, emerged loudly with the tragic event in Eastern Europe in Winter 2022, call for a fast transition to decarbonized energy sources and a dramatic reduction of the dependance on foreign energy supply, as stated in the new REPoweringEU program of the European Union. In this framework, distributed generation (DG) powered by renewable energy sources (RESs) are assets of choice [7–10]. DG includes small generation plants and energy storage systems located near users and capable of: 1) providing support to the medium voltage distribution grid which they are connected to; 2) reducing the losses associated with electricity delivery along transmission and distribution lines [11]. In such an innovative energy generation and delivery paradigm electricity flows are no longer unidirectional (or hierarchical) but bidirectional, because of local energy generation and storage, in addition to consumption. This paradigm materializes in smart grids, where information and communication technologies manage optimal energy flows [12,13] and consumer contribute to electricity generation with their own RES systems, thus acting as prosumers [14]. The above concept is implemented also in local grids capable of working autonomously as microgrids [15–17], namely, electric systems capable of interconnecting users and distributed generation sources within a defined perimeter, acting as a single controllable entity with respect to the grid (i.e., the national electricity system) [18,19]. A microgrid has the ability to operate both connected to the grid and disconnected from it, in the “off–grid” or “islanded” mode. In such a system, it is pivotal that generation, storage and user units are connected not only from an electrical point of view, but also at information level through the Energy Management System (EMS) that interacts with Power Management Systems (PMSs) of the grid key units [20–22]. In order to meet the user demand while in the islanded mode, the microgrid must operate in full autonomy ensuring an adequate level of power quality, i.e., stable frequency and voltage and low harmonic content, which involves a smart interaction between EMS and PMSs [23–25]. In some contexts, a microgrid is designed to work exclusively in islanded mode, with no connected to the grid, e.g. in remoted areas [26]. Microgrids are becoming increasingly popular not only because of their performance and control capacity, but also thanks to their advantages from the economic and environmental points of view [27, 28]. In particular, low–impact microgrids, which include generation from RESs and energy storage systems (ESSs) are progressively spreading driven by: 1) environmental sustainability of the energy supply from decarbonized sources; 2) cost decrease RESs (e.g. photovoltaic and wind power plants) and of ESSs; 3) development of intelligent control systems, which allow the management of power flows toward users and ESSs, resulting in reduced costs of energy supply; 4) importance in the electrification of rural areas in developing countries [29–31].

In the framework of such evolution, the Italian Ministry for the Environment and the Protection of the Territory and the Sea (MATTM) and the Municipality of Venice (Italy) signed an agreement on 29 December 2010 for the implementation of low–impact renewable pilot plants in the Certosa Island of the Venetian Lagoon and in the area of Fusina–Marghera, in Venice mainland. The latter consisted in a redevelopment project of a compromised industrial site, where Veritas (Veneziana Energia Risorse Idriche Territorio Ambiente Servizi) SpA was appointed to build a multi–technology pilot plant, with financial support from MATTM [32]. The plant, called *GPLab*, had to include advanced facilities for the production of energy from renewable sources and innovative energy–related technologies (Fig. 1). *GPLab* is now built and in operation. Few examples of the implemented pilot systems are outlined hereafter. A prototype green chemistry system produces biofuels based on a photobioreactor that enhances the growing of microalgal strains collected and selected from the Venetian lagoon and marine environment. These microalgae can then be used to generate biodiesel, hydrogen, biogas, and bioethanol. The PHOENIX–P2G project converts electricity into a gaseous fuel, such as methane, by means of bacteria and ultrasound, to experiment an alternative energy storage technology. A $CO_2$ supercritical system absorbs microalgal lipide that is used in biodiesel production through a transesterification process. All these pilot systems intend to promote "green" industrial development and to demonstrate that green economy can be profitable, although often overlooked by conventional chemical engineering at present [33].

The *GPLab* is powered by by a microgrid fed from RESs and ESSs, namely a 730–kW photovoltaic system (PV), while a 170–kW third–generation biodiesel generator fed from waste oils and microalgae is planned. The microgrid includes four ESSs based on different technologies: a Li–ion battery rated 300 kW and 171 kWh, a So–Ni–Cl battery rated 60 kW and 128 kWh, a Pb–A battery rated 40 kW and 101 kWh, and a electrolyzer–hydrogen–fuel cell (ELHFC) rated 20 kW and 34 kWh [32]. A fifth ESS using all–vanadium flow battery is planned. All these power units are connected to the 3–phase 400 V AC bus. Hydrogen is involved in three units of the *GPLab*, namely the electrolyzer-hydrogen- fuel cell (ELHFC) that constitutes the hydrogen energy storage system (HESS), the pilot unit extracting hydrogen from biodiesel and a pilot multidrive vessel powered by a fuel cell fed with hydrogen. This paper is focused on HESS. In Section 2 a detail description of

HESS is given and in Section 3 a brief introduction to the control strategies of the microgrid is presented. Section 4 reports the performance of the whole HESS and Section 5 presents the operation data of HESS and his components, with a focus on efficiency.

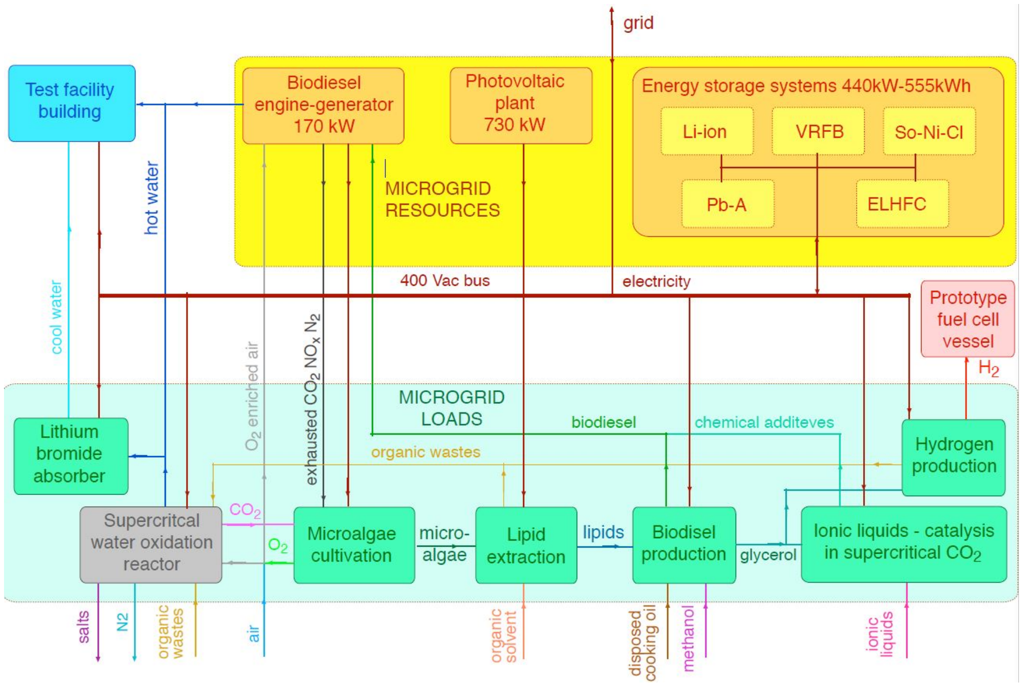


**Fig. 1 –** Schematic of the Veritas microgrid at the *GPLab* in Venice. Colors have the following meanings: azure are the local services (building lighting, conditioning, …); orange/yellow are the power sources of the microgrid consisting of a photovoltaic system (PV) and energy storage systems (ESSs); green/gray are the loads of the microgrid, consisting of carbon–free low–emissions pilot technologies; and red represents a prototype multidrive vessel powered by a fuel cell fed with the hydrogen generated in the lab. The red lines represent the 3–phase 400 V AC microgrid bus, where all units are connected in parallel. Courtesy of IEEE – Industrial Electronic Magazine [32].

## 2. Hydrogen energy storage system (HESS) architecture

A typical hydrogen energy storage system performs three fundamental operations [34–36]:

1. generates hydrogen and oxygen from pure water by consuming electric energy;
2. compresses and stores this hydrogen, while oxygen is usually released in the air;
3. generates electric energy by converting hydrogen and (atmospheric) oxygen into pure water.

In the case of the Veritas HESS, it was decided to install the devices which perform these operations in three containers, one for each operation (Fig. 2), provided with anti–salt filters to segregate the devices from the coastal brackish air and ensure durable performance. In addition, three containers limit fault propagation and allow climatizing independently the devices. Fig. 3 shows the HESS process flow diagram. The first container (Fig. 3a) houses the hydrogen generation unit (HGU), where water is demineralized and supplied to an electrolyzer (EL) generating hydrogen that undergoes a three–step purification. The HGU components and operations are detailed in Section 2.1. The second container (Fig. 3b) houses the compression and storage unit (CSU), where hydrogen is compressed and stored. The CSU components and operations are detailed in Section 2.2. The third container (Fig. 3c) houses the electric generation unit (EGU), where hydrogen and filtered air are supplied to a fuel cell (FC) and the generated electric power is conditioned for grid connection by a DC–AC inverter. A part of the heat of the water produced by the FC is recovered by a heat exchanger to perform a combined heat and power (CHP) generation. The EGU components and operations are detailed in Section 2.3.


**Fig. 2 –** *GPLab* and HESS: a) a satellite view of the laboratory (source: Google Maps); b) laboratory building; c) Convert: hydrogen generation unit (HGU), where hydrogen is generated and purified; d) Store: compression and storage unit (CSU); e) Power: electric generation unit (EGU).

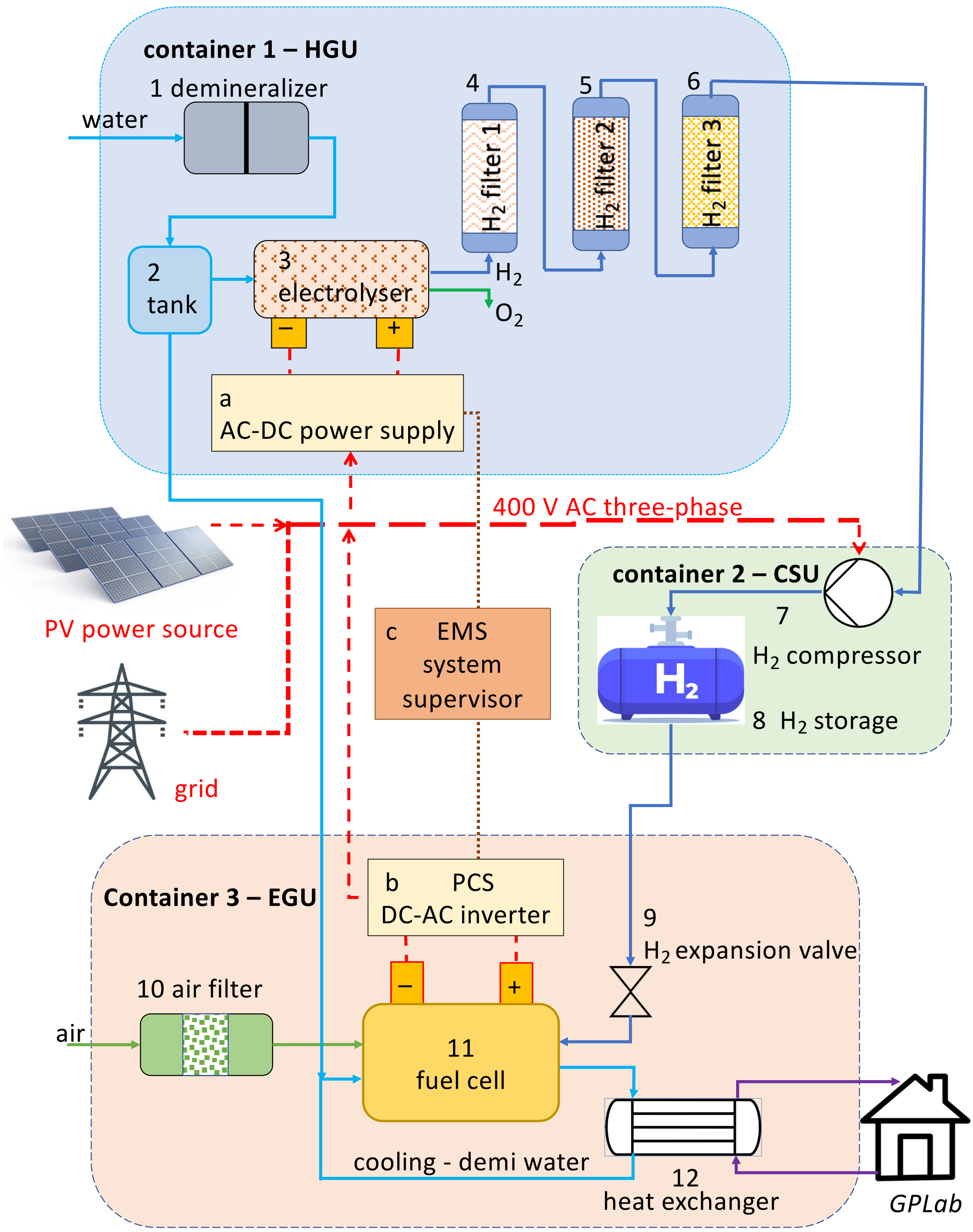


**Fig. 3 –** HESS process flow diagram: container 1 houses the Hydrogen Generation Un it (HGU), consisting of a water demineralizer (1), a water tank (2), an electrolyzer (3), a three–stages $H_2$ filter (4,5,6) and a AC–DC power supply fed from the microgrid busbar (a); container 2 houses the Compression and Storage Unit (CSU), consisting of a gas booster compressing hydrogen to 200 bar (7) and a storage system made of four tanks (8); container 3 houses the Electric Generation Unit (EGU) consisting of an expansion valve (9), an air filter (10), a fuel cell (11), a heat exchanger (12) and a DC–AC inverter feeding the microgrid busbar (b). A microgrid Energy Management System (EMS) supervises the whole process (c).

## 2.1 Container 1 – Hydrogen generation unit (HGU)

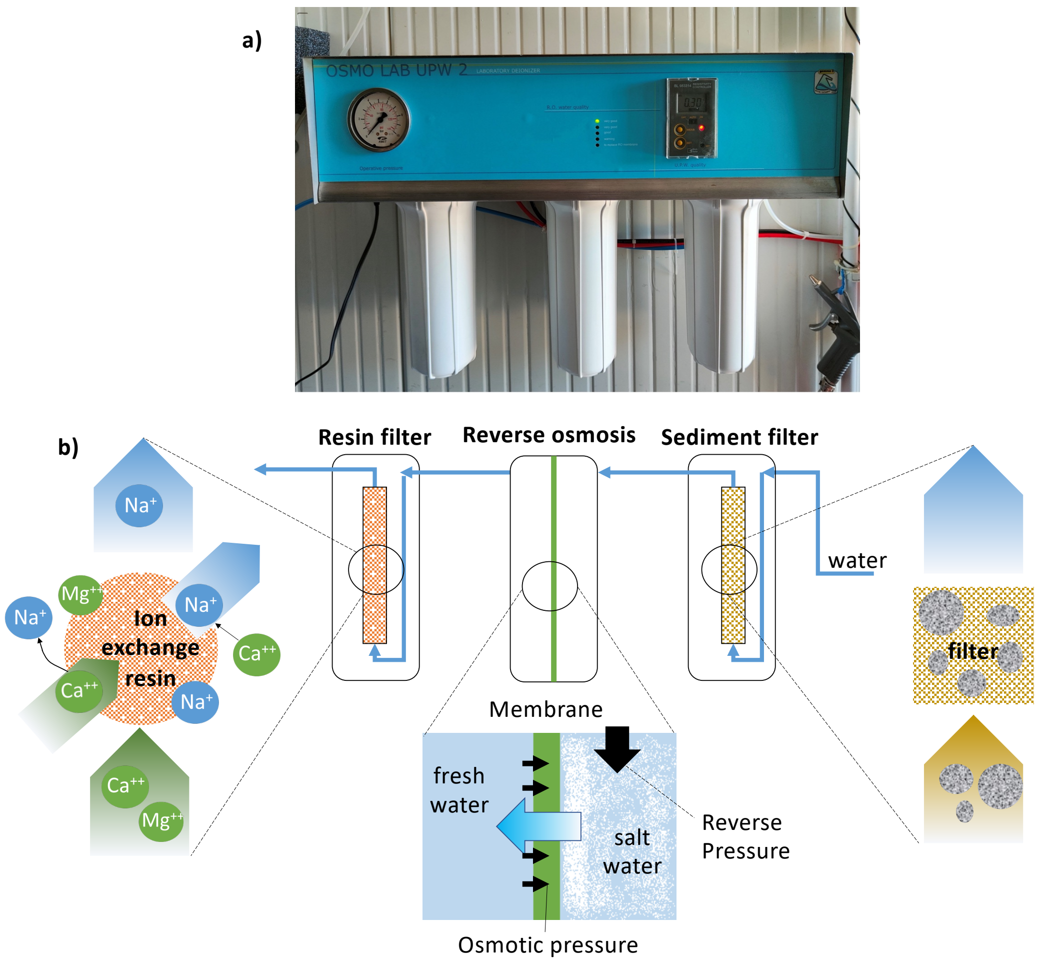


**Fig. 4** – HGU (container 1) – Water demineralizer: a) demineralizing device; b) three–step working principle, consisting of a sediment filter blocking particles up to 10 μm in size, a reverse osmosis equipment eliminating chemical species dissolved in water, and an ion exchange resin filter removing ions hazardous for the electrolyzer active materials.

The first container houses the hydrogen generation unit (HGU) consisting of a water demineralizer, an electrolyzer (EL) and a hydrogen purifier (Fig.3a). Fig. 4 shows the demineralizer (Osmo–lab UPW 2, Tecno–lab S.r.l., Italy) that performs a three–stage water filtering. The first stage uses a sediment filter to remove particles up to 10 μm in size, because particles such as sand grains can clog the flow–channels of the electrolyzer resulting in severe damages. The second stage uses a partially permeable polymer membrane to remove any chemical species suspended or dissolved in the water, such as sodium chloride. In this process, called reverse osmosis, a reverse pressure is applied to overcome the osmotic pressure of salt water, which depends on the solute concentration according to:

$$P_{osmotic} = icRT \tag{1}$$

where $i$ is the Van't Hoff constant, $c$ is the solute concentration, $R$ is the ideal gas constant and $T$ is the temperature. In the third stage an ion exchange resin filter removes specific ions, such as calcium and magnesium, to avoid precipitation inside the electrolyzer and poisoning of its active materials. Fig. 4b shows that in such process an ion is desorbed for each ion adsorbed in the resin. In this system, sodium is the ion desorbed, which does not cause any side effect in the electrolyzer.

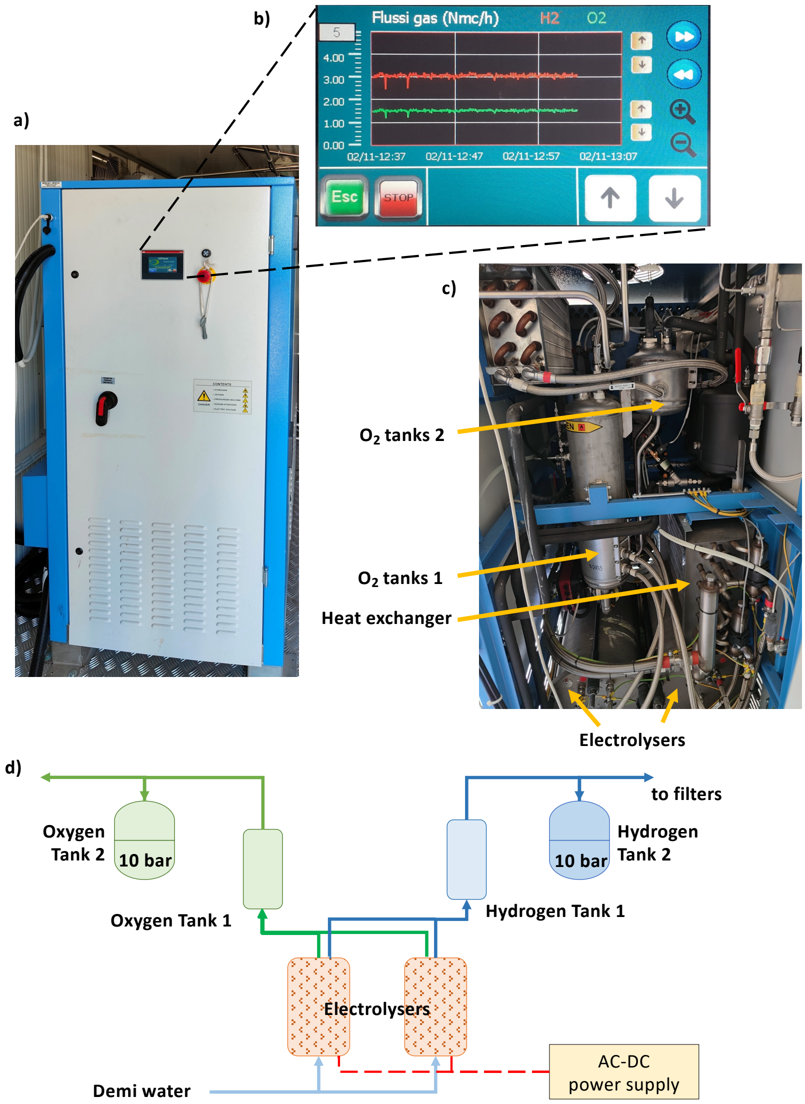


**Fig. 5 –** HGU (Container 1) – Hydrogen generating electrolyzer: a) cabinet housing two electrolyzers, four low–pressure tanks (< 10 bar), a heat exchanger and a control system; b) control panel; c) cabinet internal view revealing two electrolyzers, a heat exchanger and two oxygen tanks (two hydrogen tanks are hidden in the back); d) operating scheme of the electrolysis device.

Demineralized water is stored in a tank to be pumped into the electrolyzer (Fig. 3a). An alkaline electrolyzer (AEL) Mod. G6 by ErreDue S.p.A (Italy) was adopted that uses a potassium hydroxide (KOH) solution as electrolyte and consists of two stacks in series, each of 70 cells with an active area of 450 $cm^2$ and a power density around 0.35 W $cm^{-2}$. The electrochemical reactions which occur at the cathodes (negative poles) and anodes (positive poles) of the cells forming the stacks are respectively [37]:

$$4H_2O + 4e^- \rightarrow 2H_2 + 4OH^- \qquad E_c^0 = -0.83\ \text{V} \qquad \text{vs SHE} \tag{2}$$

$$4OH^- \rightarrow O_2 + 2H_2O + 4e^- \qquad E_a^0 = +0.40\ \text{V} \qquad \text{vs SHE} \tag{3}$$

and the overall reaction is:

$$2H_2O \rightarrow 2H_2 + O_2 \qquad E_{cell}^0 = E_c^0 - E_a^0 = -1.23\ \text{V} \qquad \text{vs SHE} \tag{4}$$

Water electrolysis in hydrogen and oxygen is an unspontaneous endothermal reaction, as attested by the negative cell potential of the overall reaction (4), which takes place only if energy is supplied. To this aim, the AEL is powered by an AC–DC power supply (PS) fed from the 3–phase 400 V AC microgrid bus, which forms the AEL unit (ELU) together with the EL. The manufacturer datasheet reports that the Mod. G6 AEL unit consumes a rated electrical power of 22.3 kW in producing a rated hydrogen flowrate of 4 $Nm^3\ h^{-1}$ [38]. The efficiencies $\eta_{EL}$ of the EL, $\eta_{PS}$ of the PS and $\eta_{ELU}$ of the whole electrolyzer unit ELU (EL+PS) are:

$$\eta_{ELU} = \frac{P_{EL-H2}}{P_{PSin}} = \eta_{EL}\,\eta_{PS} \qquad \text{with} \qquad \eta_{EL} = \frac{P_{EL-H2}}{P_{ELel}} \quad , \quad \eta_{PS} = \frac{P_{PSout}}{P_{PSin}} \tag{5}$$

where $P_{EL\text{-}H2}$ is the lower heating value (LHV) rate of the generated hydrogen, $P_{ELel}$ is the electric power consumed by the EL, $P_{PSout} = P_{ELel}$ is the electric power delivered by the PS to the EL, and $P_{PSin}$ is the electric power consumed by the PS. Given the nominal values provided in the datasheet (reported above) and a $H_2$ *LHV* = 33.322 Wh/kg, a nominal value $\eta_{ELU}$=54% results. By assuming a reasonable $\eta_{PS}$ = 90%, $\eta_{EL}$=60% is deduced for the sole electrolyzer, which is a pretty good figure for industrial EALs. According to the manufacturer information, $\eta_{PS}$ and $\eta_{EL}$ are increasing and decreasing functions of the operating power, respectively, and their combined effects result in a $\eta_{ELU}$ increasing with power [39]. A heat exchanger (Fig. 5c) fed with internally released heat supplies the electrolyzer to keep its temperature in an optimal range of 50–60 °C. Generated hydrogen and oxygen are temporarily stored in two tanks (tank 1 and tank 2 in Fig. 5). When the gas pressures in these tanks reach of 10 bars, oxygen is vented out while hydrogen is moved to the purifier.

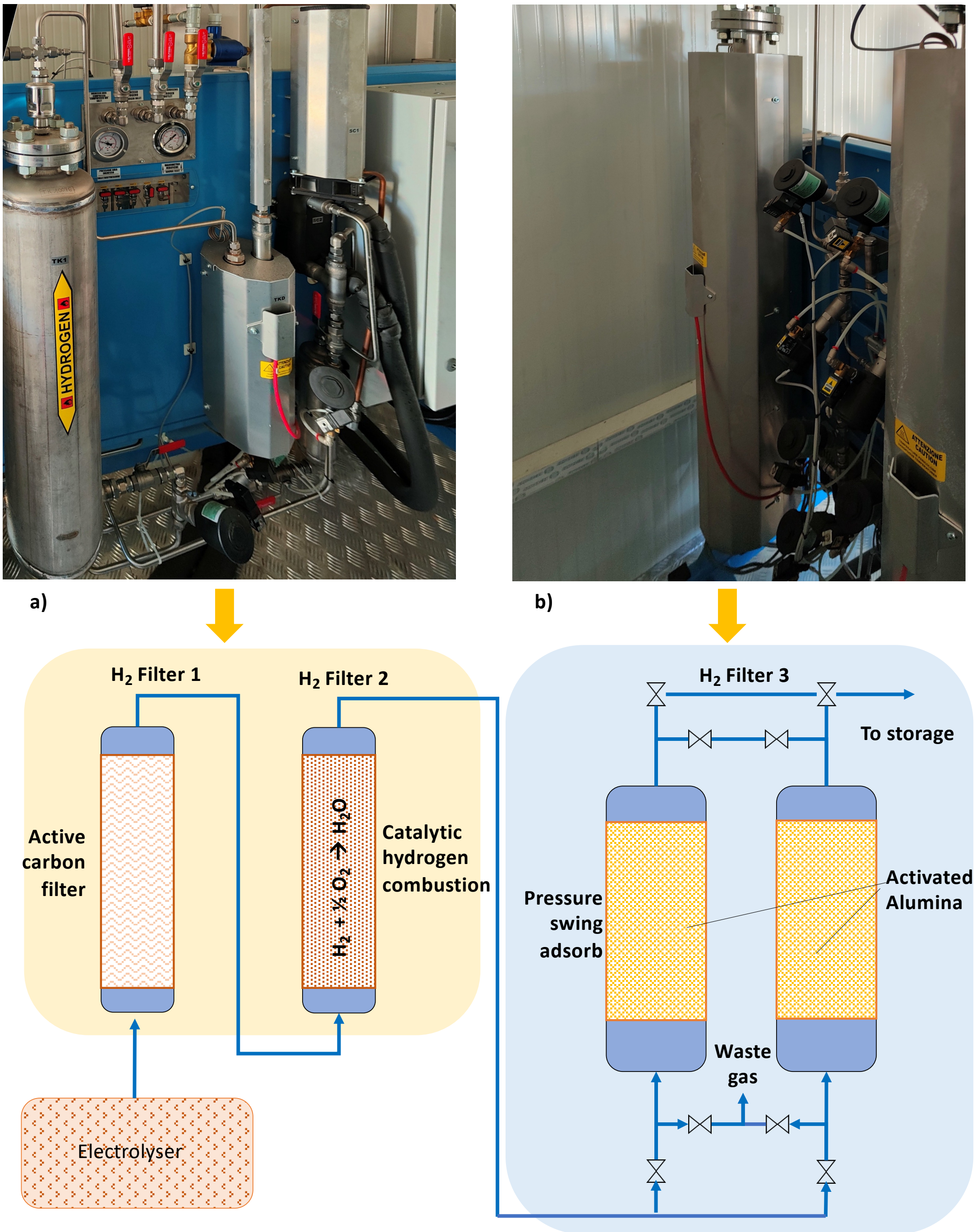


**Fig. 6 –** HGU (Container 1) – Three-stage hydrogen purifier. Picture a) stage 1: gas filter with active carbon and stage 2: reactor for catalytic hydrogen combustion eliminating any traces of other gases (e.g., oxygen) and consuming 8% of hydrogen. After this stage a chiller cools down the gas at circa 5 °C. Picture b) stage 3: two columns providing the pressure swing adsorption process with activated alumina eliminating any traces of water resulting from hydrogen combustion. A dew point of –70 °C is reached. After the filtering process, hydrogen presents a purity level of 99.9998%.

The hydrogen generated by the EL is processed by the purifier to remove oxygen, water vapor and other gases to a purity of 99.9998%. This high figure is obtained through the three–stage process shown in Fig.

6. In the first stage an active carbon filter captures different gases, such as carbon dioxide ($CO_2$) and carbon monoxide (CO), which can poison the FC active materials, notably the precious–metal catalyzers. The second purifying stage consists of a catalytic hydrogen combustion (CHC), performing the reaction [40]:

$$2H_2 + O_2 \rightarrow 2H_2O\ (g) \qquad \Delta H_r^0 = -241.8 \text{ kJ mol}^{-1} \tag{6}$$

This strongly exothermal reaction eliminates molecular oxygen ($O_2$) from hydrogen. Different catalysts can be used, and most of them are Pt–based catalysts, which allow that this combustion takes place at low temperature (in the range 35–90 °C), improving the safety and the controllability of the process [40]. The reaction takes place in a plug flow reactor (PFR) sized to trigger a self–fed process when the electrolyzer reaches about 8% of its nameplate power. 8-10% of the hydrogen is burned in this reaction while a chiller cools down the remaining outlet hydrogen to 5 °C. The third stage is a pressure swing adsorption (PSA) process activated with alumina which ensures an optimal hydrogen drying, removing the steam produces in the electrolysis. Alumina is contained in two adsorption columns which work alternatively: in one column alumina adsorbs the steam while in the second column it undergoes a regeneration process that reactivates it for the next adsorption. This third stage provides a hydrogen dew point of –70 °C, suitable for compressing hydrogen at a pressure of 200 bar in the storing tanks with no condensation.

Water demineralizer and its pump, hydrogen purifier with chiller and container ancillaries have their power consumption $P_{ADD1}$ that adds to the ELU consumption to give the total consumption $P_{HGU} = P_{PS\text{-}in} + P_{ADD1}$ of the HGU in container 1. In addition, due to the hydrogen burned in the purification process, a larger hydrogen quantity must be produced respect to the stored one. Correspondingly, the efficiency $\eta_{HGU}$ of the HGU is lower than the efficiency $\eta_{ELU}$ of the ELU expressed in eq. (5) and can be derived from this expression by substituting $P_{PSin}$ with $P_{HGU}$ and the $P_{EL\text{-}H2}$ with $P_{HGU\text{-}H2}$:

$$\eta_{HGU} = \frac{P_{HGU-H2}}{P_{HGU}} = \eta_{ELU}\eta_{ADD1} \quad \text{with} \quad \eta_{ADD1} = \frac{P_{PSin}}{P_{HGU}}\frac{P_{HGU-H2}}{P_{EL-H2}} = \frac{P_{PSin}}{P_{PSin}+P_{ADD1}}\frac{P_{EL-H2}-P_{H2comb}}{P_{EL-H2}} \tag{7}$$

where $\eta_{ADD1}$ is the efficiency related to the HGU additional devices, clearly lower than 100%. Similar expressions hold for the energy efficiencies of a whole process of energy storage, provided that the energies

$W$, i.e. time integrals of powers $P$, replace powers. If the operation is managed at constant powers, such energy efficiencies equate the corresponding power efficiency.

### 2.2 Container 2 – Compression and Storage Unit (CSU)

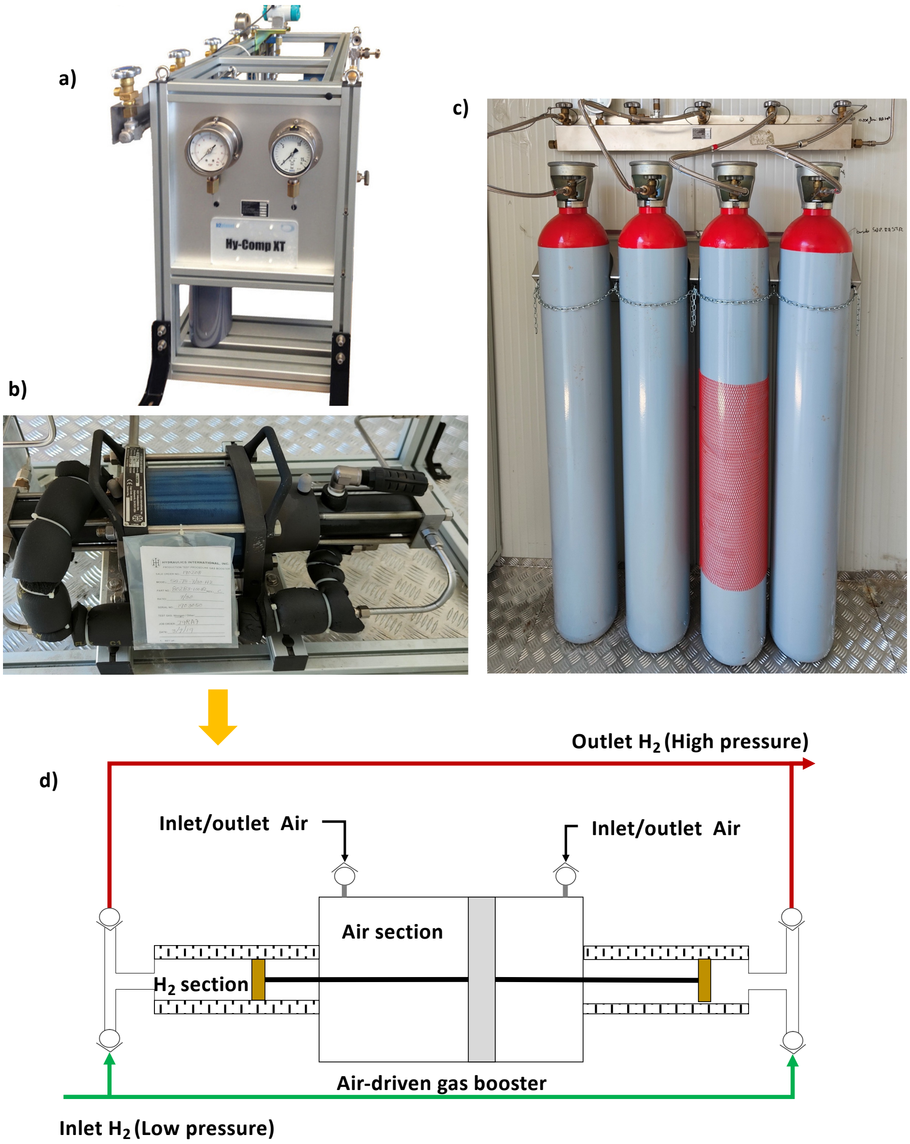


**Fig. 7 –** CSU (Container 2) – Storage system: a) standard Hy–COMP XT HP skid for analog signals controlling the compression of hydrogen at the air–driven gas booster; b) air–driven gas booster; c) storage tanks with a total volume of 200 L; d) schematic of the air–driven gas booster.

The second container houses the compression and storage unit (CSU) (Fig. 7). Compression is produced by an air–driven gas booster (Hydraulics International, INC., USA) namely a double–action piston pump in which a large piston, powered by low–pressure compressed air, drives two reciprocating slim pistons compressing hydrogen at a pressure up to 220 bar (Fig. 7d). A Hy–COMP XT HP skid (H2planet, Italy) driven by a programmable logic controller (PLC) controlling the inlet and outlet booster pressures via voltage–free contacts and analog signals to regulate the gas flow rate up to 3.1 $Nm^3\ h^{-1}$. High–pressure hydrogen is stored in an array of four 50-L cylinders capable of 220 bar, fed through a valved manifold connected to the gas booster (Fig. 7c). In operation, the hydrogen pressure in the tanks is actually kept between 40 bar and 200 bar, resulting in a storage capacity of 200 L at 200 bar and a depth of discharge DoD = 80%. The lower limit ensures a proper and efficient FC operation, while the upper limit constitutes a safety margin with respect to the 220-bar tank maximum value. The mass of hydrogen produced and stored in the tanks can be calculated by the Van der Waals equation of state [41]:

$$P = \frac{nRT}{V-nb} - a\frac{n^2}{V^2} \quad \text{with} \quad a = \frac{27}{64}\frac{R^2T_c^2}{P_c} \quad , \quad b = \frac{RT_c}{8P_c} \tag{8}$$

where $P$ is the pressure, $V$ is the volume, $T$ is the temperature, $R$ =8.314 J $mol^{-1}$ $K^{-1}$ is the ideal gas constant and $n$ are the moles of hydrogen. $T_c$ = 33.19 K and $P_c$ = 1.313 MPa are the hydrogen critical temperature and critical pressure, respectively. Table 1 reports the quantity of hydrogen stored in the four tanks at different operating pressures, taken from the manufacturer datasheet.

**Tab.1: Quantity of hydrogen stored in the four tanks at different operating pressures**

| **Pressure [bar]** | 10 | 50 | 100 | 150 | 200 | 220 |
|---|---|---|---|---|---|---|
| **Quantity [$Nm^3$]** | 1.86 | 9.08 | 17.62 | 25.66 | 33.22 | 36.11 |

Considering the hydrogen lower heating value LHV = 33.322 Wh/kg, 33.22 $Nm^3$ ($m$ = 2.93 kg) of hydrogen stored at the maximum operating pressure of 200 bar contains the stored energy $W_{H2}$ = 99.43 kWh, [41]. In the compression process, the quantity and thus the energy $W_{H2} = W_{HGU\text{-}H2}$ of the stored hydrogen do not change from the value delivered by the HGU, but the energy $W_{CSU}$ used in compressing the gas in the CSU increases further the power demand of the storage process $W_{in} = W_{CSU} + W_{HGU}$. Correspondingly, the efficiency $\eta_{STO}$ of the whole storage system (HGU+CSU) is lower than the efficiency $\eta_{HGU}$ of EGU expressed in eq. (7) and can be derived from this expression by substituting $W_{HGU}$ with $W_{in}$:

$$\eta_{STO} = \frac{W_{HGU-H2}}{W_{in}} = \eta_{HGU}\,\eta_{CSU} \quad \text{with} \quad \eta_{CSU} = \frac{W_{HGU}}{W_{in}} = \frac{W_{HGU}}{W_{HGU}+W_{CSU}} \tag{9}$$

where $\eta_{CSU}$ is the efficiency of the CSU, clearly lower than 100% due to the consumption in the compressor and auxiliaries. More generally, all efficiencies considered in eqs. (5), (7) and (9) imply that every phase and component of the $H_2$ storage process shrinks the overall efficiency.

### 2.3 Container 3 – Electric Generation Unit (EGU)


a) b)

**Fig. 8 –** EGU (Container 3) is divided in two zones, hosting the PEM fuel cell system and the DC–AC inverter: a) PEMFC with the air filtering device and heat exchanger; b) DC–AC inverter and the electrical switchboard forming the power conditioning system (PCS).

The third container houses the electric generation unit (EGU) and is divided in two compartments, one hosting an expansion valve that reduces the hydrogen pressure in a dissipative process, the FC, its air filtering system and heat exchanger, and the other compartment hosting the power conditioning system (PCS) and the electric switchboard and connection to the 3–phase 400 V AC microgrid bus (Fig. 8). The FC is a PEM type (PEMFC) HyPM®HD30 by Hydrogenics (CAN) that uses proton–exchange membranes (PEMs) as an electrolyte and consists of 120 cells with an active area of ca. 19 cm × 40 cm. It works on hydrogen and air which are fed at a pressure of 10 bars, the latter being filtered to prevent catalyst poisoning from coastal brine.

The electrochemical reactions taking place at the cell anodes (negative poles) and cathodes (positive poles) are respectively:

$$2H_2 \rightarrow 4H^+ + 4e^- \qquad E_a^0 = 0\ \text{V} \quad \text{vs SHE} \tag{10}$$

$$O_2 + 4H^+ + 4e^- \rightarrow 2H_2O \qquad E_c^0 = +1.23\ \text{V} \quad \text{vs SHE} \tag{11}$$

and the overall reaction is:

$$2H_2 + O_2 \rightarrow 2H_2O \qquad E_{cell}^0 = E_c^0 - E_a^0 = +1.23\ \text{V} \quad \text{vs SHE} \tag{12}$$

The efficiency $\eta_{FC}$ of a FC is:

$$\eta_{FC} = \frac{P_{FCel}}{P_{FC-H2}} \tag{13}$$

where $P_{FC-el}$ is the electric power delivered by the FC and $P_{FC-H2}$ is the lower heating value (LHV) energy rate of the consumed hydrogen. Due to internal losses, this efficiency decreases with increasing the load current (and power) [39]. The HyPM®HD30 datasheet reports a maximum electrical power of 33 kW and a nominal (maximum) efficiency of 53% at 9 kW, that reduces at 37.7% at maximum power [42]. Since 1.5 kW of the generated electric power are consumed in internal FC services, the FC delivered electric power is $P_{FC-el}$=31.5 kW. The exothermal reaction (12) produces an entropic thermal power $W_{FC-heat}$ = 52 kW, that is removed by means of a cooling circuit fed with demineralized water. About 67% of this power is recovered and used in air conditioning the *GPLab* in a combined heat and power (CHP) generation that raises the overall FC CHP efficiency at full power to 73.6%. A DC–AC inverter operates as PCS of interface to the grid, i.e. manages the stack power flow by stepping up the 60–120 V DC stack voltage and converting it to 3–phase 400 V AC. The manufacture datasheet reports a maximum efficiency $\eta_{PCS}$ = 89.3% at an input power $P_{PCSin}$ = 11.2 kW that gradually reduces at 84.1% at the maximum input power $P_{PCSin}$ = 31.5 kW, so that the maximum power delivered is $P_{PCSout}$ = 26.5 kW, given its efficiency $\eta_{PCS}$:

$$\eta_{PCS} = \frac{P_{PCSout}}{P_{PCSin}} \tag{14}$$

Since the inverter is fed with the net power generated by the FC, $P_{PCSin} = P_{FCel}$, the efficiency $\eta_{FCU}$ of the whole FC unit FCU (FC+PCS) is:

$$\eta_{FCU} = \frac{P_{PCSout}}{P_{FC-H2}} = \eta_{FC}\ \eta_{PCS} \tag{15}$$

Given the PEMFC and PCS rated values reported above, eq. (15) implies that the FCU delivers a maximum power $P_{PCSout}$ = 26.5 kW at maximum FC power $P_{FCel}$ = 31.5 kW, with an electric efficiency $\eta_{FCU}$ = 31.7%. The power $P_{ADD3}$ consumed by the fluid-circulation pumps reduces the generated power to give the net released power $P_{out} = P_{PSCout} - P_{ADD3}$ of the EGU in container 3. Correspondingly, the efficiency $\eta_{EGU}$ of the EGU is lower than the efficiency $\eta_{FCU}$ of the FCU shown in eq. (15) and it can be derived from this expression by substituting $P_{IPCSout}$ with $P_{out}$:

$$\eta_{EGU} = \frac{P_{out}}{P_{FC-H2}} = \eta_{FCU}\eta_{ADD3} \qquad \text{with} \qquad \eta_{ADD3} = \frac{P_{out}}{P_{PCSout}} = \frac{P_{PCSout} - P_{ADD3}}{P_{PCSout}} \tag{16}$$

where $\eta_{ADD3}$ is the efficiency related to the EGU additional devices, clearly lower than 100%. Also in this case, similar expressions hold for the energy efficiencies of a whole process of energy delivery, provided that the energies *W*, i.e. the time integrals of powers *P*, replace powers. In an operation managed at constant powers, such energy efficiencies equate the corresponding power efficiency.

## 3. HEES Control

Since the HESS is included in the microgrid of the *GPLab*, it is operated together with the other microgrid power systems by a central control system, the energy management system (EMS), that incorporates advanced strategy to guarantee high levels of reliability and efficacy [32]. Major issues for the safe operation of the microgrid include: 1) maintaining the stability of the microgrid to minimize the probability of failures, interruptions and blackouts; 2) control voltage and frequency in the any critical operating modes (such as off–grid, black start, grid connection, etc.; 3) managing bidirectional power flows within the microgrid; 4) minimizing the operating costs of the energy source; 5) synchronizing the microgrid with the grid (connected mode); 6) managing the power flows between microgrid and while purchasing/selling electricity from/to the grid based on actual prices of the electricity market. To ensure flexible and effective operation, the control system of a microgrid must include: 1) a telecommunication system that interconnects all the microgrid systems; 2) data systems capable of efficiently producing and exchanging data and measurements; 3) advanced control algorithms; 4) decision support and human interface.

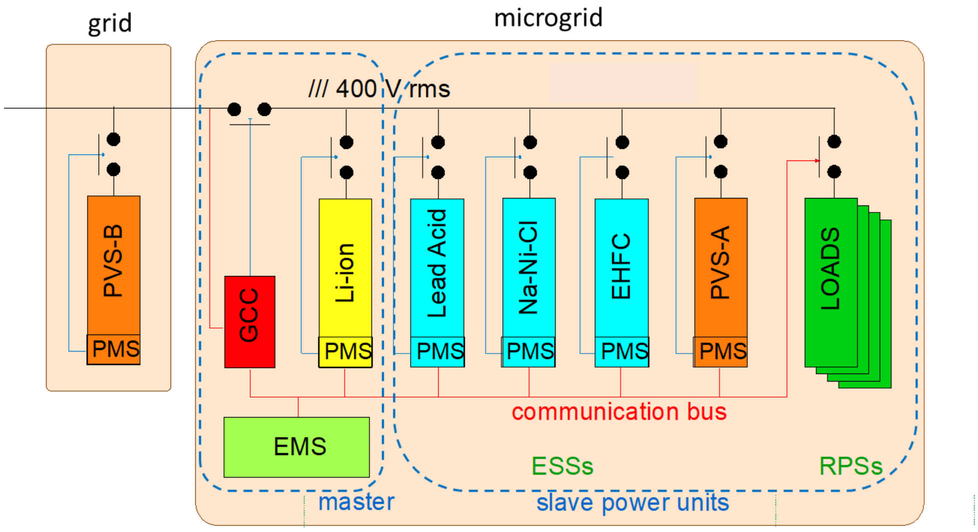


**Fig. 9 –** Hierarchical structure of the microgrid highlighting the master PMS, the slave PMSs, the PMS dedicated to grid connection and the EMS. Courtesy of IEEE – Industrial Electronic Magazine [32].

To perform these tasks, the *GPLab* microgrid uses a 3–level hierarchical architecture with an Energy Management System (EMS) at top level and Power Management System (PMS) in each system (RESs and ESSs) at medium level [31–32]. Since all units are connected in parallel to the microgrid bus (Fig. 9), only one PMS acts as a master system, while all the others, including HEES, act as slave systems, thus avoiding instabilities and critical conditions to the microgrid. The master system is the PMS of the 300-kW Li–ion ESS, which can operate in two ways, i.e. as a voltage source when the microgrid is islanded (off–grid mode) supplying the bus voltage reference to all slave systems and as a current source when the microgrid is connected to the grid (on–grid mode) that provides the voltage reference to the microgrid. All slave ESSs operate as current sources, in both off–grid and on–grid modes. The control logic conforms a hierarchical structure, alike its physical architecture, following the different importance and needed timing of the control functions. Accordingly, the HESS PMS performs autonomously a primary level control, which uses local measurements, reacts immediately to local events with predefined action, and does not require any communication. In addition, the HESS PMS commands secondary and tertiary level actions, under the control of the EMS.

## 4 HESS nominal performance

In the implemented configuration described in Section 2 and in the framework of the microgrid control architecture described in Section 3, the HESS provides the following functions and performance:

1. it consists of three main units housed in three independently climatized containers allowing to apply differentiated climate control aimed at optimized unit operation;
2. generates and compresses up to 3.1 $Nm^3\ h^{-1}$ of 99.9998% pure hydrogen;
3. stores 200 L of hydrogen at a pressure up to 200 bar;
4. provides brine–free air to the FC to ensure long operative life;
5. generates electric power up to 26.5 kW;
6. discharges the stored hydrogen down to 40 bar, reaching a depth of discharge (DOD) of 80%;
7. recovers 35 kW of thermal power from the FC and uses it in a CHP process to air conditioning the *GPLab* building;
8. allows remote control of both hydrogen and electricity generation from the microgrid EMS for a flexible and efficient management of the HEES.

Table 2 summarizes the nominal data of the units forming the HESS, as provided by the manufacturers.

**Tab.2: Technical data of the main units and components of the HESS as stated by manufacturers**

| | **Values** | **Units** |
|---|---|---|
| **Water demineralizer** | | |
| Demi water consumed | 4 | $L\ h^{-1}$ |
| Demi water quality | 5 | $\mu S\ cm^{-1}$ |
| **Electrolyzer (EL) and AC–DC power supply** | | |
| Maximum hydrogen flow rate | 4 | $Nm^3\ h^{-1}$ |
| Maximum consumed power | 22.3 | kW |
| Noisiness | 72 | db |
| **Hydrogen purifier** | | |
| Work pressure | 10–12 | bar |
| Dew point of outlet $H_2$ | –70 | °C |
| Consumed power | 2.70 | kW |
| **Compressor** | | |
| Inlet $H_2$ pressure | 8–12 | bar |
| Maximum outlet $H_2$ pressure | 220 | bar |

| | | |
|---|---|---|
| Operative outlet $H_2$ pressure | 200 | bar |
| Hydrogen flow rate | 3.1 | $Nm^3 h^{-1}$ |
| Consumed power | 7.5 | kW |
| **Fuel cell (FC)** | | |
| Current | 0–500 | A |
| Voltage | 60–120 | V |
| Nominal (gross) electric power | 33.0 | kW |
| Net maximum electric power | 31.5 | kW |
| Maximum electric efficiency at 27% of max power | 53.0 | % |
| Electric efficiency at nominal power | 37.7 | % |
| Maximum generated thermal power | 52.0 | kW |
| Temperature of the outlet cooling liquid | 50–70 | °C |
| **DC–AC Inverter** | | |
| Input voltage | 5–200 | V DC |
| Input current | 0–500 | A DC |
| Output voltage | 400 | V AC |
| Maximum input power | 31.5 | kW |
| Maximum output power | 26.5 | kW |
| Maximum electric efficiency at 28.5% of max power | 89.3 | % |
| Electric efficiency at 100% full power | 84.1 | % |

### 4.1 HESS instrumentation

The instrumentation of the HESS allows monitoring, control and testing the whole system. Power analyzers QNA500 by Asita srl (Italy) measure the voltage, current, and electric power exchanged by the containers which house the subsystems HGU, CSU and EGU and provide relevant figures including active, reactive, apparent powers, power factor, and active and reactive energies at a precision of ±0.2% in compliance with ISO50001, ISO14001 and IEC 62053-22 standards. Hydrogen flow rates in HGU and EGU are computed from the EL and FC electric currents via the stoichiometry of reactions (2) and (10), respectively. A Siemens Pressure Transmitter 0-400 Bar 4-20 mA measures the pressure of the hydrogen produced in the HGU. Two thermometers by Fimet provide the cooling water temperatures at the inlet and outlet of the FC heat exchanger at a precision of ±2 °C while the cooling water flow rate in the heat exchanger is provided by Grundfos Magna3 electronically controlled pumps. From these last measurements the FC thermal power is computed.

### 4.2 HESS Round trip efficiency

A round-trip operation consists in an energy charge-discharge cycle in which: a) a hydrogen mass *m* containing the energy $W_{H2} = m$ LHV is generated, compressed, and stored (; b) the same hydrogen mass *m* is discharged to release its stored energy. Since the same hydrogen mass *m* generated in charge is used in discharge, $W_{H2}$ corresponds to the energy $W_{HGU-H2}$ of eq. (7) and to the energy $W_{FC-H2}$ consumed by the FC at the rate $P_{FC-H2}$ of eq. (13). In the charging process the overall consumed electrical energy $W_{CH} = W_{in}$ is provided by the grid and, by applying eqs. (5), (7) and (9), the charge efficiency results:

$$\eta_{CH} = \frac{W_{H2}}{W_{CH}} = \eta_{EL}\,\eta_{PS}\,\;\eta_{ADD1}\;\,\eta_{CSU} \tag{17}$$

In the discharge process the same stored energy $W_{H2}$ is discharged to the grid through the FC and PCS, at the net of the auxiliary consumption $W_{DIS}$=$W_{out}$ at the rate $P_{out}$ of eq. (15). By applying eqs. (13), (14), (15) and (16), the discharge efficiency results:

$$\eta_{DIS} = \frac{W_{DIS}}{W_{H2}} = \eta_{FC}\,\eta_{INV}\,\eta_{ADD3} \tag{18}$$

The round-trip efficiency RTE of a whole charge-discharge cycle of a storage system in the ratio between the net energy released in discharge and the total energy consumed in charge. By combining eqs. (17) and (18), the RTE results:

$$\eta_{RT} = \frac{W_{DIS}}{W_{CH}} = \eta_{DIS}\eta_{CH} = \eta_{EL}\,\eta_{PS}\,\eta_{ADD1}\;\,\eta_{CSU}\,\eta_{FC}\,\eta_{INV}\,\eta_{ADD3} \tag{19}$$

all factors forming the right-hand side being lower than 100%. In the case of a CHP operation, the heat produced by the FC and recovered $W_{FCheat}$ adds to the net released electric energy $W_{DIS}$ and the *RTE* becomes:

$$\eta_{RT-CHP} = \frac{W_{DIS}+W_{FCheat}}{W_{CH}} = \eta_{RT} + \frac{W_{FC-heat}}{W_{CH}} \tag{20}$$

## 5. HESS operation

The HESS has undergone test campaigns to assess its performance. Operations were run in steady state conditions, thus avoiding the issues which may arise from highly dynamic operations [29]. Experimental profiles of the electric power exchanged in the HGU+CSU and EGU together with stored energy and state of charge (SOC) in a typical operation are reported in Fig. 10. SOC is here defined as the ratio between the available and the maximum hydrogen stored moles $n/n_M$, namely, in isothermal conditions, the ratio between the actual and nominal hydrogen pressures, so that SOC=100% indicates a tank pressure of 200 bar. The *x*-axis indicates the time needed to charge/discharge from 40 bar to 200 bar and vice versa. The charge process is carried out at an average consumed power of 29,03 kW over 12.5 hours (Fig.10a), consuming a total energy of 363 kWh (Fig.10c). Although the ELU generation potentiality is 4 $Nm^3\ h^{-1}$, the charge process was run at 3.1 $Nm^3\ h^{-1}$ due to bottleneck flow rate of the compressor. A slowdown in the compressor operation at ca. 500 minutes is shown. After charge, the EGU operated for 1.2 hours to discharge the tanks from 200 bar back to 40 bar, generating an average power of 26.5 kW (Fig.10b) and an electric energy of 31.53 kWh (Fig.10d). Taking the ELU system at steady power required ca. 25 min.

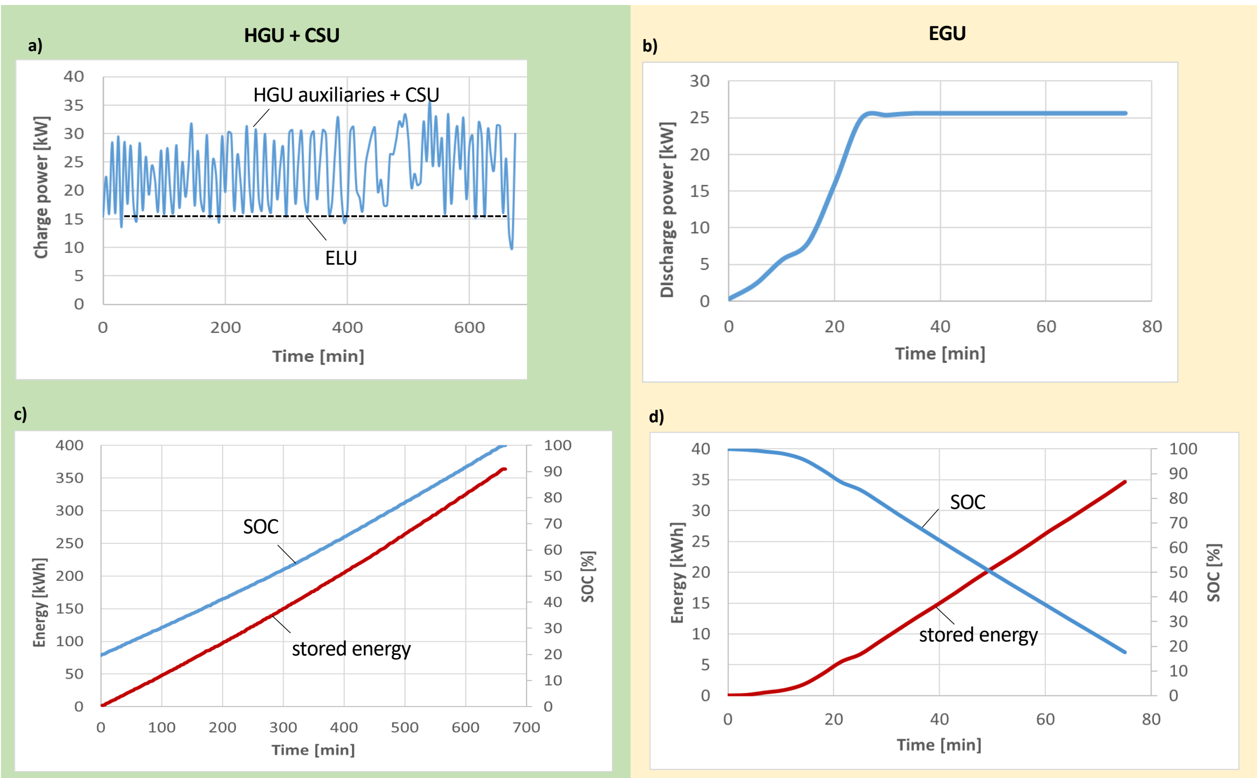


**Fig.10** – Experimental power and energy profiles during a typical charge–discharge cycle. a) Electric power consumed by the HGU+CSU in hydrogen production and storage – fluctuations are mainly due to the high-pressure compressor; b) electric power produced by the EGU during discharge; c) electric energy consumed by the HGU+CSU in an energy storage process SOC from 20% to 100% (hydrogen pressure from 40 bar to 200 bar); d) electric energy generated by the EGU during a discharge process with SOC from 100% to 20% (hydrogen pressure from 200 bar to 40 bar).

**Tab.3: Summary table of the performance of the HESS during average operation and nominal conditions.**

| Item | Units | Nominal values | Experimental values |
|---|---|---|---|
| **Hydrogen Generation Unit – HGU** | | | |
| $H_2$ flow rate | $Nm^3 h^{-1}$ | 4.0 | 3.1 |
| $H_2$ energy flow rate | kW | 12.0 | 9.28 |
| ELU consumed power | kW | 22.3 | 17.5 |
| ELU efficiency | % | 54.0 | 52.9 |
| Duration of charging operation | h | 9.6 | 12.5 |
| ELU consumed energy | kWh | 215 | 225 |
| $H_2$ purifier consumed energy | kWh | 29.6 | 54.4 |
| Generated hydrogen volume | $Nm^3$ | 38.6 | 38.6 |
| Generated hydrogen energy | kWh | 115.6 | 115.6 |
| Net hydrogen volume | $Nm^3$ | 33.22 | 33.22 |
| Net hydrogen energy | kWh | 99.43 | 99.43 |
| HGU efficiency | % | 40.7 | 35.6 |
| **Compression and Storage Unit – CSU** | | | |
| $H_2$ flow rate | $Nm^3 h^{-1}$ | 3.1 | 3.1 |
| Energy consumed in $H_2$ compression | kWh | 78.4 | 78.4 |
| Energy consumed by auxiliary items | kWh | 4.6 | 4.6 |
| Compressed hydrogen volume | $Nm^3$ | 33.22 | 33.22 |
| Compressed hydrogen energy | kWh | 99.43 | 99.43 |
| CSU efficiency | % | 54.5 | 54.5 |
| **Electric Generation Unit – EGU** | | | |
| Supplied hydrogen energy | kWh | 99.43 | 99.43 |
| PEMFC net generated electric power | kW | 31.5 | 31.5 |
| PEMFC electric efficiency at maximum power | % | 37.7 | 37.7 |
| Duration of discharging operation | h | 1.2 | 1.2 |
| PEMFC generated electric energy | kWh | 37.5 | 37.5 |
| DC–AC Inverter efficiency at maximum power | % | 84.1 | 84.1 |
| Electric energy generated by the FCU | kWh | 31.5 | 31.5 |
| PEMFC generated useful thermal power | kW | 35.0 | 35.0 |
| PEMFC generated useful thermal energy | kWh | 41.6 | 41.6 |
| Energy consumed by auxiliary items | kWh | 1.25 | 1.25 |
| Energy efficiency of EGU – electric only | % | 31.3 | 31.3 |
| Energy efficiency of EGU – CHP mode | % | 72.7 | 72.7 |
| **HESS – RTE – Cycle efficiency (electric only)** | % | 9.2 | 8.7 |
| **HESS – RTE – Cycle efficiency (CHP)** | % | 21.3 | 20.1 |

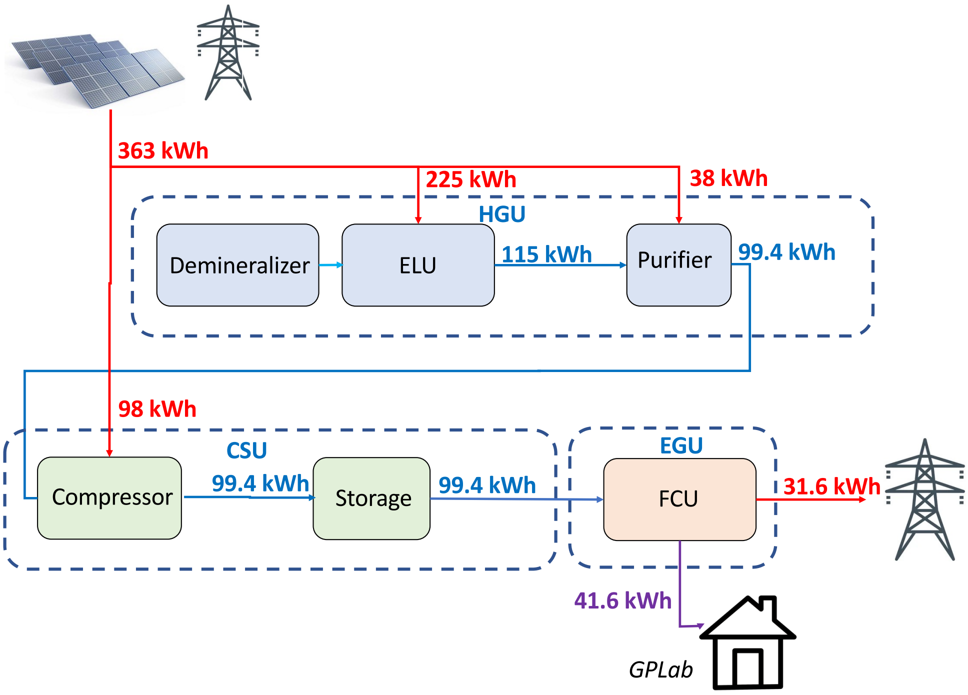


**Fig.11** – Energy flow diagram of the HESS in normal operating condition.

Measured and deduced performance value of the system devices and of the whole HESS in a typical operation are reported in Tab. 3, whereas fig.11 shows an energy flow diagram. The experimental efficiencies were obtained from devices datasheets or computed from the energy measurements, based on the expressions given in the previous equations. The RTE efficiency was computed as the ratio between the net energy delivered by the EGU (either electric or electric plus heat) and the total energy consumed by the HGU and CSU according to eqs. (19) and (20). In the charge phase, 33.22 Nm$^3$ of hydrogen (containing 99.43 kWh of energy) were generated, compressed, and stored, and to obtain this outcome 225 kWh were consumed in the ELU, 55 kWh in the purifier and auxiliaries and 83 kWh in the compression unit, which sum up to ca. 363 kWh. The energy efficiency of the ELU was 52.9% and the energy efficiency of the whole HGU was 35.6%. Compression and storage resulted particularly energy consuming, with an efficiency of 54.5%. In the discharge phase, the FCU generated an electrical energy of 31.53 kWh at an efficiency of 31.7%. Due to other internal consumption, the EGU efficiency resulted in 31.3%. In addition, 41.6 kWh of thermal energy were recovered and used for air conditioning in a CHP mode, that raised the EGU efficiency of 72.7%. As a result of such charge/discharge operation, the round-trip efficiency (RTE) of the HESS resulted of 8.7% in the electric mode and 20.1% in the CHP mode. The different charge and discharge times, 12.5 h and 1.2 h, respectively, depend partially on the different operating power of the EL and FC, ca. 20 kW and 33 kW, respectively, and mostly on the low RTE of the HESS, which implies $W_{out}$ =8.7% $W_{in}$. Some further comments on the system efficiency are worthwhile. Just considering the maximum efficiency of the electrolyzer $\eta_{EL}$=60% and of the fuel cell $\eta_{FC}$=53%, a purely theoretical efficiency of the electricity-hydrogen-electricity process $\eta_{RT}$=31.8% can be deduced. By considering the two devices operated at nominal power ($\eta_{EL}$=57.3% and $\eta_{FC}$=37.7%) this figure reduces to $\eta_{RT}$=21.6%. However, EL and FC do not work without their power supply and power conditioning system, and when we account for the efficiency of these PS and PCS, considering $\eta_{ELU}$=52.9% and of $\eta_{FCU}$=31.7%, the RTE reduces further to $\eta_{RT}$=16.8%. In addition, a real system EL needs that water is demineralized, hydrogen purified and compressed and FC fluids be flown. When all the energy consumed by these devices are also taken into account, the RTE drops to $\eta_{RT}$=8.7%.

**5. Conclusions**

In this work, a hydrogen energy storage system included in microgrid of the *GPLab* of Veritas S.p.A. is presented. This HESS consists of three units. The first one, HGU, includes a water demineralizer, a 22.3-kW AEL and a three–step purifier providing hydrogen with 99.9998% purity. The second unit, CSU, includes an air–driven gas booster for compressing hydrogen in four tanks with a total storage capacity of 33.22 $Nm^3$ at 200 bar. The third unit, EGU, includes a 33–kW PEMFC stack, an air filtering and blowing system, a heat exchanger recovering the FC thermal power and a DC–AC inverter managing the power flow toward the grid. Each unit is installed in a container provided with air filtering and conditioning. In nominal condition the alkaline electrolyzer produces a hydrogen flowrate of 4 $Nm^3h^{-1}$ at a maximum efficiency of 60% and the PEM fuel cell produces 33 kW of electric power, having a maximum efficiency of 55% at reduced power. However, these efficiencies reduce significantly in normal operation at nominal power and energy is also consumed by electric power interfaces and ancillaries of the ESS, including water filtering, hydrogen purification and compression, fluid flow. As a result, the nominal efficiency of the HESS drops to 8.7%. By recovering 35 kW of the thermal power produced by the FC in a CHP generation, the nominal efficiency of the HESS rises to 20.1%. It must be said that the system here presented is not fully optimized, despite resorting to top-quality components. Just to mention one issue, a solid oxide fuel cell (SOFC) can provide an efficiency 10%–12%

higher than a PEMFC [43], while requiring less pure hydrogen, so that purification and compression are simpler and less energy demanding, and producing at the same time high-temperature entropic heat, which can be better recovered in a CHP operation. That said, the experimental results here presented evidence that it is unrealistic to qualify the performance of a HESS by means of a theoretical efficiency given by the multiplying the top electrolyzer and fuel cell efficiencies, as it is sometimes claimed for this type of energy storage systems, because they require a number of energy-consuming devices and components. Secondly, the electric round-trip efficiency of a better optimized HESS would range around 20%, that is a quite modest figure if compared to other ESSs. More technological development is needed to bring hydrogen energy storage to better performance, but a large gap is likely to remain with respect to other electrochemical energy storage systems (namely, batteries) some of which can even offer power/energy independency, which is a main feature of a HESS.

## 6. Acknowledgments

AB acknowledges financial support from MATTM (the Italian Ministry for Environment and Land and Sea Protection) and the Venetian Municipality. NP and MG acknowledge financial support from the project "Grid–optimized vanadium flow batteries: architecture, interconnection and economic factors" (GUAR_RICERCALASCITOLEVI 20_01), within the 2019 Research Program of the Interdepartmental Centre Giorgio Levi Cases for Energy Economics and Technology of University of Padua and from the project "Holistic approach to EneRgy–efficient smart nanOGRIDS – HEROGRIDS" within (PRIN 2017 2017WA5ZT3) within the Italian MUR 2017 PRIN program.

## References

[1] M. Liserre, T. Sauter, J. Y. Hung, Future energy systems: Integrating renewable energy sources into the smart power grid through industrial electronics, IEEE Ind. Electron. Mag., 2010;4:18–37. http://dx.doi.org/10.1109/MIE.2010.935861.

[2] M. Beaudin, H. Zareipour, A. Schellenberglabe, W. Rosehart, Energy storage for mitigating the variability of renewable electricity sources: An updated review, Energy Sustain. Develop., 2010;14;302–314. http://dx.doi:10.1016/j.esd.2010.09.007.

[3] A. Evans, V. Strezov, and T. J. Evans, Assessment of utility energy storage options for increased renewable energy penetration, Renew. Sust. Energ. Rev., 2012;6;4141–4147. http://doi.org/10.1016/j.rser.2012.03.048.

[4] X. Luo, J. Wang, M. Dooner, and J. Clarke, Overview of current development in electrical energy storage technologies and the application potential in power system operation, Appl. Energy, 2015;137;511–536. https://doi.org/10.1016/j.apenergy.2014.09.081.

[5] N. Günter and A. Marinopoulos, Energy storage for grid services and applications: Classification, market review, metrics, and methodology for evaluation of deployment cases, J. Energy Storage, 2016; 8;226–234. https://doi.org/10.1016/j.egypro.2018.08.119.

[6] Conference of the Parties COP26, "COP26 declaration on accelerating the transition to 100% zero emission cars and vans," Glasgow, 10.11.2021, https://ukcop26.org/cop26–declaration–on–accelerating–the–transition–to–100–zero–emission–cars–and–vans/; [accessed 10/11/2021].

[7] T. Ackermann, G. Andersson, and L. Söder, Distributed generation: A definition, Electr. Power Syst. Res., 2001;57;195–204. https://doi.org/10.1016/S0378–7796(01)00101–8.

[8] G. Marbán, T. Valdés-Solís, Towards the hydrogen economy?, Int. J. Hydrog. Energy, 2007;32;1625-1637. http://doi.org/10.1016/j.ijhydene.2006.12.017.

[9] I.P. Jain, Hydrogen the fuel for 21st century, Int. J. Hydrog. Energy, 2009; 34; 7368-7378. http://doi.org/10.1016/j.ijhydene.2009.05.093.

[10] K.J. Dillman, J. Heinonen, A 'just' hydrogen economy: A normative energy justice assessment of the hydrogen economy, Renew. Sust. Energ. Rev., 2022;167;112648, https://doi.org/10.1016/j.rser.2022.112648.

[11] E. J. Coster, J. M. A. Myrzik, B. Kruimer, and W. L. Kling, Integration issues of distributed generation in distribution grids, Proc. IEEE, 2011;99;28–39. http://doi.org/10.1109/JPROC.2010.2052776.

[12] A. Ipakchi, F. Albuyeh, Grid of the future, IEEE Power Energy Mag., 2009; 7; 52–62. http://doi.org/10.1109/MPE.2008.931384.

[13] P. Siano, Demand response and smart grids – A survey, Renew. Sust. Energ. Rev., 2014;30;461–478. http://doi.org/10.1016/j.rser.2013.10.022.

[14] R. Zafar, A. Mahmood, S. Razzaq, W. Ali, U. Naeem, K. Shehzad, Prosumer based energy management and sharing in smart grid, Renew. Sust. Energ. Rev., 2018;82;1675–1684. http://doi.org/10.1016/j.rser.2017.07.018.

[15] W. Xie, X. Xia, Distributed Energy Dispatch of Electrical Energy Storage Systems Using Consensus Control Approach, IFAC-PapersOnLine,2018;51;229234. https://doi.org/10.1016/j.ifacol.2018.07.283.

[16] B. Shakerighadi, S. Peyghami, A New Guideline for Security Assessment of Power Systems with a High Penetration of Wind Turbines, Appl. Sci., 2020;10;3190. https://doi.org/10.3390/app10093190.

[17] J. Cho and A. N. Kleit, Energy storage systems in energy and ancillary markets: A backwards induction approach, Appl. Energy, 2015;147;176–183. https://doi.org/10.1016/j.apenergy.2015.01.114.

[18] M. Müller, L. Viernstein, C. N. Truong, A. Eiting, H. C. Hesse, R. Witzmann, and A. Jossen, Evaluation of grid–level adaptability for stationary battery energy storage system applications in Europe, J. Energy Storage, 2017;9;1–11. https://doi.org/10.1016/j.est.2016.11.005.

[19] C. Patsios, B. Wu, E. Chatzinikolaou, D. J. Rogers, N. Wade, N. P. Brandon, and P. Taylor, An integrated approach for the analysis and control of grid connected energy storage systems, J. Energy Storage, 2016;5;48–61. https://doi.org/10.1016/j.est.2015.11.011.

[20] E. Hossain, E. Kabalci, R. Bayindir, and R.Perez, Microgrid testbeds around the world: State of art, Energy Convers. Manag., 2014;86;132–153. https://doi.org/10.1016/j.enconman.2014.05.012.

[21] W. F. Pickard, A. Q. Shen, and N. J. Hansing, Parking the power: Strategies and physical limitations for bulk energy storage in supply–demand matching on a grid whose input power is provided by intermittent sources, Renew. Sust. Energy Rev, 2009;13;1934–1945. https://doi.org/10.1016/j.rser.2009.03.002.

[22] B. Dunn, H. Kamath, and J. Tarascon, Electrical energy storage for the grid: A battery of choices, Science, 2011;334; 928–935. https://doi.org/10.1126/science.1212741.

[23] J. Kondoh, I. Ishii, H. Yamaguchi, A. Murata, K. Otani, K. Sakuta, N. Higuchi, S. Sekine, and M. Kamimoto, Electrical energy storage systems for energy networks, Energy Convers. Manag., 2000;41; 1863–1874. https://doi.org/ 10.1016/S0196–8904(00)00028–5.

[24] B. P. Roberts and C. Sandberg, The role of energy storage in development of smart grids, Proc. IEEE, 2011; 99;1139–1144. https://doi.org/10.1109/JPROC.2011.2116752.

[25] A. Zucker and T. Hinchliffe, Optimum sizing of PV–attached electricity storage according to power market signals—A case study for Germany and Italy, Appl. Energy, 2014;127;141–155. https://doi.org/10.1016/j.apenergy.2014.04.038.

[26] M. R. Aghamohammadi and H. Abdolahinia, A new approach for optimal sizing of battery energy storage system for primary frequency control of islanded microgrid," Elect. Power Energy Syst., 2014;54;325–333. https://doi.org/10.1016/j.ijepes.2013.07.005.

[27] S. P. Chowdhury, S. Chowdhury, and P. A.Crossley, Islanding protection of active distribution networks with renewable distributed generators: A comprehensive survey, Electric Power Syst. Res., 2009;6; 984–992, 2009. https://doi.org/10.1016/j.epsr.2008.12.012.

[28] D. Ipsakis, S. Voutetakis, P. Seferlis, F. Stergiopoulos, C. Elmasides, Power management strategies for a stand-alone power system using renewable energy sources and hydrogen storage, (2009) Int. J. Hydrog. Energy, 2009;34; 7081-7095. http://doi.org/10.1016/j.ijhydene.2008.06.051.

[29] P. Fragiacomo, E. Astorino, G. Chippari, G. De Lorenzo, W. T. Czarnetzki, W. Schneider, Dynamic modeling of a hybrid electric system based on an anion exchange membrane fuel cell, Cogent Engineering, 2017;4;1357891. https://doi.org/10.1080/23311916.2017.1357891.

[30] F. Katiraei, M. R. Iravani, and P. W. Lehn, Micro–grid autonomous operation during and subsequent to islanding process, IEEE Trans. Power Del., 2005;20;248–257. https://doi.org/10.1109/TPWRD.2004.835051.

[31] F. Blaabjerg, R. Teodorescu, M. Liserre, and A.V. Timbus, Overview of control and grid synchronization for distributed power generation systems, IEEE Trans. Ind. Electron., 2006;53;1398–1409. https://doi.org/10.1109/TIE.2006.881997.

[32] M. Guarnieri, A. Bovo, A. Giovanelli, P. Mattavelli, A Real Multitechnology Microgrid in Venice, IEEE Ind. Electron. Mag., 2018;19–31. https://doi.org/10.1109/MIE.2018.2855735.

[33] L. Mario Pastore, G. Lo Basso, M. Sforzini Livio de Santoli, Technical, economic and environmental issues related to electrolysers capacity targets according to the Italian Hydrogen Strategy: A critical analysis, Renew. Sust. Energ. Rev., 2022, 166;112685. https://doi.org/10.1016/j.rser.2022.112685.

[34] O. Schmidt, A. Gambhir, I. Staffell, A. Hawkes, J. Nelson, S. Few, Future cost and performance of water electrolysis: An expert elicitation study, Int. J. Hydrog. Energy, 2017; 42; 30470-30492. http://doi.org/10.1016/j.ijhydene.2017.10.045.

[35] F. Zhang, P. Zhao, M. Niu, J. Maddy, The survey of key technologies in hydrogen energy storage, Int. J. Hydrog. Energy, 2016; 41;14535-14552. http://doi.org/10.1016/j.ijhydene.2016.05.293.

[36] O. Ulleberg, T. Nakken, A. Eté, The wind/hydrogen demonstration system at Utsira in Norway: Evaluation of system perfromance using operational data and update hydrogen energy system modeling

tools, International J. Hydrog. Energy, 2010;35;1841–1852. https://doi.org/10.1016/j.ijhydene.2009.10.077.

[37] W.R.W. Daud, R.E. Rosli, E.H. Majlan, S.A.A. Hamid, R. Mohamed PEM fuel cell system control: a review Renew Energy, 2017;113. https://doi.org/10.1016/j.renene.2017.06.027.

[38] ErreDue SpA Technical Gases on Site, Operating Manual, Livorno, Italy, 20/04/2003, Rev. 25/03/2016.

[39] M. Guarnieri, P. Alotto, F. Moro, Modeling the Performance of Hydrogen-Oxygen Unitized Regenerative Proton Exchange Membrane Fuel Cells for Energy Storage, J. Power Sources, 297 (11), (2015) 23-32. https://doi.org/j.jpowsour.2015.07.067.

[40] V.N. Nguyen, Study of the catalytic combustion of lean hydrogen–air mixtures in monolith reactor, Int. J. Hydrog. Energy, 2018;43;17520–17530. https://doi.org/10.1016/j.ijhydene.2018.07.126.

[41] J.R. Elliott, C. T. Lira, Introductory chemical engineering thermodynamics, 2nd ed. New York: Prentice Hall; 2012.

[42] Hydrogenics, HyPM®HD30, Product Manual, Revision 8, October 2018.

[43] V. Cigolotti, M. Genovese, P. Fragiacomo, Comprehensive Review on Fuel Cell Technology for Stationary Applications as Sustainable and Efficient Poly-Generation Energy Systems, Energies, 2021, 14, 4963. https://doi.org/10.3390/en14164963.